

# Efficient and accurate strategy for high-fidelity simulations of solid rocket motor ignition

*Laurent François*<sup>†</sup>, *Joël Dupays*<sup>\*</sup>, *Marc Massot*<sup>\*\*</sup>

<sup>\*</sup>*ONERA - The French Aerospace Lab, Palaiseau, France*

<sup>\*\*</sup>*CMAP - École Polytechnique, Palaiseau, France*

laurent.francois@onera.fr · joel.dupays@onera.fr · marc.massot@polytechnique.edu

<sup>†</sup>Corresponding author

## Abstract

A framework is presented for the simulation of ignition transients in solid rocket motors. The methodology is based on the coupling of a CFD solver for the combustion chamber flow field and a 1D solver for the unsteady combustion of the propellant, locally at each propellant boundary face of the CFD domain. Two approaches are presented. The first one solves the propellant flame in 1D, encapsulating all the numerical and multiscale modelling difficulties (surface processes, kinetics for the flame) within the boundary model. The second approach captures the propellant flame within the fluid model of the multidimensional CFD solver, while only the surface and solid phase thermal profile are solved in 1D within the boundary model. Both approaches are compared for the laser-induced ignition of a propellant in 1D, and on a discriminating 2D test case where a propellant surface is impinged by a hot igniter jet flow. The results compare very favourably, showing that accounting for the propellant flame only in the boundary model yields accurate ignition dynamics.

## 1. Introduction

Being able to accurately simulate the ignition transient of a solid rocket motor (SRM) is of paramount importance for the design of efficient and reliable propulsion systems. Since more than 50 years, various models and tools of increasing complexities have been developed to tackle this issue. Early volume-filling models [1, 2] failed at capturing the unsteady gas flow dynamics and progressive ignition of the propellant grain. Later 1D models improved those aspects [3, 4], however ignition in complex geometries could only be captured via ad hoc corrections. Fully 3D models accounting for the true geometry of the combustion chamber have therefore emerged in the 1990s [5, 6] to enable an accurate reproduction of the internal flow dynamics, e.g. pressure waves, recirculations. The 3D modelling involves the proper resolution of the conjugate heat transfer (CHT) between the propellant surface and the igniter gas flow before ignition, a problematic that already involves many difficulties and is still the subject of a large research effort [7, 8]. Compared to the CHT framework for inert materials, the solid propellant case adds multiple complexities: transition from an inert surface to a reactive one, strong heat release from the propellant flame in a very thin zone above the propellant surface (typically a few hundred micrometers thick), parietal mass injection.

The knowledge of the surface dynamics, propellant flame chemistry and structure has progressed a lot but is still incomplete. Detailed propellant combustion solvers (1D to 3D) are very computationally intensive [9, 10, 11, 12] and cannot be considered for the simulation of a complete motor. Consequently, all the reported 3D approaches use a simplified modelling of the propellant ignition and combustion [13, 14, 15]. The solid propellant, initially acting as an inert material, is heated up by convective and radiative heat fluxes from the gas phase. The unsteady evolution of the combustion chamber flow field is computed by a CFD solver. The thermal profile in the solid propellant is assumed one-dimensional locally at each boundary face and its unsteady evolution is coupled with the gas flow at regular intervals, allowing for a time-accurate simulation of the ignition transient. Once a propellant boundary face reaches a predefined ignition temperature, instantaneous ignition is assumed and the boundary model switches to quasi-steady burning (Vieille law).

Several fundamental issues arise from the classical simplified modelling. First, using an ignition temperature criterion is approximate and cannot easily account for the dependence of this temperature on the heat

## SOLID ROCKET MOTOR IGNITION MODELLING

flux history or other factors [16]. Second, assuming instantaneous ignition, i.e. transition from inert heating to quasi-steady burning, automatically discards dynamic burning effects where the burn rate temporarily exceeds its steady-state value due to excessive pre-heating. Third, the propellant flame (be it explicitly modelled with analytical transient models [17], or conceptually hidden in semi-empirical burn rate laws) has a size on the order of 0.1-1 mm which means that it may well overlap with the first cells of the chamber CFD mesh. Potential flame-flow interactions, e.g. erosive burning can only be accounted for by using empirical correction factors. Fourth, all the combustion models for large-scale ignition simulations use a quasi-steady propellant flame. Transient flame dynamics, e.g. flame establishment, may thus be inaccurate. Finally, no study has been presented to investigate the dependence of the computed ignition dynamics on the CFD mesh refinement, in particular for the accuracy of the wall heat transfer and the propagation of ignition.

In the present work, we introduce two approaches for the simulation of motor ignition. They offer a more detailed modelling of the ignition transient and of the propellant combustion, enabling a better understanding of the previously mentioned effects. The first model captures the propellant flame entirely within the CFD solver, with a refined CFD mesh near the surface, avoiding the previous assumption of one-dimensionality for the flame. A 1D model of solid propellant thermal profile and surface processes is used as boundary model. This detailed approach allows for an accurate depiction of the propellant flame establishment and its interaction with the combustion chamber flow field. This approach is intractable for large-scale 3D simulations, however 2D simulations are possible. The second model, inspired by the previous ignition models from ONERA [17, 18], is similar, except the propellant flame is also modelled in 1D within the boundary model. Compared to the previous analytical transient flame models from ONERA, the gas phase combustion is solved numerically and can include detailed combustion kinetics if required, enabling more accurate characteristics to be simulated.

Both coupled approaches are confronted on two cases using simplified kinetics: solid propellant laser-induced ignition in 1D, and a discriminating 2D case with impingement of a hot igniter jet flow on a propellant surface, involving strong interactions between the flow field and the surface dynamics. Both approaches compare very favourably, indicating that the boundary model involving a 1D flame does not induce physical artefacts due to the additional modelling assumptions it involves.

## 2. Modelling

In this section, we first present the detailed modelling of the propellant combustion, where the propellant flame and the combustion chamber flow field are captured within a single fluid model, while the solid propellant thermal profile and surface are solved with a dedicated boundary model. We then introduce a one-dimensional propellant flame model as an additional layer to decrease the fluid model complexity.

### 2.1 Fluid model

The combustion chamber gas flow is modelled by the multispecies compressible Navier-Stokes equations. The  $k - \omega$  SST model [19] is added to capture turbulent effects, e.g. enhanced heat transfer. For the sake of simplicity, we only recall the laminar conservation equations for mass, species, momentum ( $j$ -th direction) and total energy  $e_t$ :

$$\frac{\partial}{\partial t} \begin{pmatrix} \rho \\ \rho Y_k \\ \rho u_j \\ \rho e_t \end{pmatrix} = \begin{pmatrix} -\frac{\partial \rho u_i}{\partial x_i} \\ -\frac{\partial \rho u_i Y_k}{\partial x_i} \\ -\frac{\partial \rho u_i u_j}{\partial x_i} - \frac{\partial P}{\partial x_j} \\ -\frac{\partial \rho u_i e_t}{\partial x_i} - \frac{\partial P \delta_{ij} u_i}{\partial x_j} \end{pmatrix} + \begin{pmatrix} 0 \\ -\frac{\partial J_{k,i}}{\partial x_i} \\ \frac{\partial \tau_{ij}}{\partial x_j} \\ -\frac{\partial}{\partial x_i} \left( -\lambda \frac{\partial T}{\partial x_i} + \sum_{k=1}^{n_e} h_k J_{k,i} \right) + \frac{\partial \tau_{ij} u_i}{\partial x_j} \end{pmatrix} + \begin{pmatrix} 0 \\ \omega_k \\ 0 \\ 0 \end{pmatrix} \quad (1)$$

The viscous stress tensor  $\tau_{ij}$  is computed as  $\tau_{ij} = 2\mu D_{ij}$  where the deviator tensor is defined as  $D = S - \frac{1}{3}tr(S)\mathbb{I}$  with  $S = \frac{1}{2}(\vec{\nabla}\vec{u} + \vec{\nabla}\vec{u}^t)$ . The mixture is composed of  $n_e$  species. The term  $J_{k,i}$  is the component in the  $i$ -th direction of the diffusion flux vector  $\vec{J}_k$  for the  $k$ -th species, evaluated with the classical Hirschfelder-Curtiss approximation. The volumetric production rate of the  $k$ -th species is  $\omega_k$ . The enthalpy  $h$  is the sum of the chemical and sensible enthalpies:  $h = \sum_{k=1}^{n_e} Y_k h_k$ , where  $h_k = \Delta h_k^0 + \int_{T_{std}}^T c_{p,k}(a) da$ , with  $c_{p,k}$  the heat capacity of the  $k$ -th species, and  $\Delta h_k^0$  its formation enthalpy at  $T_{std}$  the standard temperature. The thermal

conductivity is  $\lambda$ . The Kronecker symbol is  $\delta_{ij}$ . Soret and Dufour effects are neglected. The model does not account for gas phase and surface radiation. Finally, the ideal gas law relates the pressure  $P$  to the other variables:

$$\rho = P / \left( RT \sum_{k=1}^{n_e} \frac{Y_k}{\mathcal{M}_k} \right) \quad (2)$$

with  $\mathcal{M}_k$  the molar mass of the  $k$ -th species, and  $R$  the universal gas constant.

## 2.2 Solid propellant model

This model describes the evolution of the thermal profile within the solid propellant. Due to the insulating nature of the propellant, the thickness of the thermal profile is typically on the order of 100  $\mu\text{m}$  and is very small compared to other characteristic scales of the flow and motor. Consequently, as in most ignition models from the literature, we assume that heat diffusion only occurs in the direction normal to the surface. The thermal profile is described by the temperature field  $T(x, y, z, \eta)$ , with  $(x, y, z)$  the position of the surface point considered, and  $\eta$  the coordinate along the normal to the surface (negative towards the propellant). The propellant surface is kept at  $\eta = 0$  via a change of variable [20], which introduces a convective term in the model. The solid phase at  $\eta < 0$  is assumed semi-infinite, inert and homogeneous. In-depth thermal degradation of the propellant is not considered. The temperature field is governed by the following partial differential equation:

$$\rho_c c_c \partial_t T + \rho_c c_c r \partial_\eta T - \partial_\eta (\lambda_c \partial_\eta T) = 0 \quad (3)$$

with  $\rho_c$  the propellant density,  $c_c$  its heat capacity,  $\lambda_c$  the thermal conductivity, and  $r$  the absolute surface regression speed, deduced from Eq. (8). Far below the surface, the solid is at its resting temperature  $T_0$ .

## 2.3 Surface connection conditions

The fluid and solid models are connected at the surface of the solid propellant. In reality, this interface may be a so-called ‘‘foam’’ zone, a thin layer where liquid and gas phases coexist. However, its properties and behaviour are not well established, hence we simplify its modelling by representing this zone as an infinitely thin layer where all the pyrolysis and gasification processes occur. We use the subscript  $s$  to identify the values that are taken at the surface for the solid propellant model, i.e. at  $\eta = 0$ . The subscript  $w$  denotes the parietal (wall) values used in the fluid model, which in the case of this detailed modelling, will be identical to the values at the propellant surface model (subscript  $s$ ).

The gas and solid phases are connected through the propellant surface by considering the continuity of the mass flow rate, temperature, and by balancing enthalpy and species fluxes:

$$\begin{cases} \rho_c r = m = \rho_w \vec{u}_w \cdot \vec{n} & (4) \\ T(0^-) = T(0^+) = T_s & (5) \\ (mh - \lambda_c \partial_\eta T)_{0^-} = \vec{n} \cdot (mh \vec{n} - \lambda \vec{\nabla} T + \sum_1^{n_e} h_k \vec{J}_k)_{0^+} - \Phi_{ext} & (6) \\ (m Y_{inj,k})_{0^-} = \vec{n} \cdot (m Y_k \vec{n} + \vec{J}_k)_{0^+} \quad \forall k \in \llbracket 1, n_e \rrbracket & (7) \end{cases}$$

with  $\vec{n}$  the unit vector normal to the surface, oriented towards  $\eta > 0$  (inside of the CFD domain) and  $Y_{inj}$  the mass fractions of the products generated by the decomposition and gasification processes, which can be constants or functions of the surface temperature as in [21]. The external heat flux  $\Phi_{ext}$  may represent additional fluxes, e.g. radiative heating. The surface mass flow rate  $m$  is given by the pyrolysis law:

$$m = f(T_s, P) \quad (8)$$

We assume that gaseous species leaving the surface are injected in the direction perpendicular to the propellant boundary face. Hence, the parietal fluid velocity is perpendicular to the surface ( $\vec{u}_w \wedge \vec{n} = \vec{0}$ ) and its magnitude is such that the mass flow rate is continuous across the surface. The parietal values of the turbulent variables  $k$  and  $\omega$  are user-specified constants.

## 2.4 One-dimensional propellant flame modelling

Since the propellant flame is very thin compared to the chamber characteristic length scale ( $\approx 1$  m), it can be computationally advantageous to describe it as a smaller separate system. This discards reactions from the fluid model, and the near-surface CFD mesh can be coarsened since it does not need to capture the flame any more. 1D flame models are adequate for homogeneous propellants, and also for heterogeneous propellants over a wide range of pressures [22]. The space coordinate along the one-dimensional flame is  $\eta$  as for the solid phase, and the same change of variable is performed to track the regressing propellant surface. The flame at  $\eta > 0$  is modelled as a low-Mach reactive flow:

$$\begin{cases} \partial_t \rho + \partial_\eta(\rho(u+r)) = 0 & (9) \\ \partial_t \rho Y_k + \partial_\eta(\rho(u+r)Y_k) = -\partial_\eta J_k + \omega_k & \forall k \in \llbracket 1, n_e \rrbracket & (10) \\ \partial_t \rho h + \partial_\eta(\rho(u+r)h) = -\partial_t P - \partial_\eta(-\lambda \partial_\eta T + \sum_1^{n_e} h_k J_k) & (11) \end{cases}$$

In previous work [20, 23, 24], we have conducted extensive analysis of this flame model, demonstrating its well-posedness, its specific mathematical properties that require specific numerical methods, and its relevance for solid propellant applications.

This flame model is inserted as an additional modelling layer between the fluid and surface models. The surface connection conditions must now be applied between the solid model from Section 2.2 and the 1D flame model. The field variables of the 1D flame model replace the ones of the chamber fluid model in the right-hand sides of Eqs. (4) to (7).

New connection conditions must be provided to link the 1D flame and chamber fluid models. In practice, to ensure the propellant flame is entirely captured within the 1D flame model, the 1D domain extends much further than the typical flame height, so that chemical equilibrium is reached, allowing for the flame-related kinetics to be discarded from the fluid model. This introduces specific difficulties regarding the temporal coherence and conservativity of the coupling between the flame and fluid models, which we avoid by enforcing the quasi-steadiness of the 1D flame, setting all time derivatives in Eqs. (9) to (11) to 0. The 1D chamber fluid prescribes the value of the parietal pressure  $P_w$  as the value of the thermodynamic pressure  $P$  in the whole 1D gas domain. In return, the 1D flame model transmits flow rates of mass, species and energy. From the point of view of the fluid model, the propellant surface is still considered as an adherence surface, however the parietal values of the field variables are set to the values of the same fields at the exit of the 1D gas phase (subscript  $f$ ). Chemical equilibrium being reached within the 1D gas phase, the exit boundary conditions for the 1D flame are simple Neumann conditions:

$$\partial_\eta T(+\infty) = 0, \quad \partial_\eta Y_k(+\infty) = 0 \quad \forall k \in \llbracket 1, n_e \rrbracket \quad (12)$$

Therefore, no diffusive fluxes leave the 1D flame model, only convective fluxes. To ensure physical coherence of the coupling, surface species diffusion fluxes are set to 0 for the fluid model as well. Due to the previous modelling choices, the conjugate heat transfer between the fluid model and solid models cannot be captured by the 1D flame model. It must be handled by reintroducing a direct connection between the fluid and solid models. This is done by inserting the wall heat flux from the fluid model into the surface coupling condition (6). This wall heat flux is computed as:

$$\Phi_w = \lambda \vec{\nabla} T \cdot \vec{n} = (\lambda \partial_\eta T)_w \quad (13)$$

We stress that the temperature field used in this last equation is the one of the fluid model, not the 1D flame. The heat flux is evaluated at the surface, i.e. for  $\eta = 0$ . It is conveniently added in Eq. (6) by setting  $\Phi_{ext} = \Phi_w$ . Note that we do not include surface friction power, since its contribution is usually 3 to 5 orders of magnitude lower than that of heat conduction.

## 3. Coupled framework for SRM ignition simulations

To simulate the previous models, we choose to avoid a monolithic approach where all the models are solved within one single solver. Instead, we capitalize on software already developed at ONERA, only requiring the specific surface coupling conditions to be implemented. In this section, we present the various solvers and the coupling procedure.

The fluid model for the combustion chamber flow field is implemented in the CFD solver CHARME of the multiphysics simulation toolchain CEDRE from ONERA [25]. It relies on a cell-centered finite volume

technique on general unstructured meshes. The convective fluxes are computed with the HLLC approximate Riemann solver and a second-order multislope MUSCL scheme [26], while diffusive fluxes are evaluated with a second-order centered scheme. For the temporal discretisation, several linearised implicit Runge-Kutta methods can be applied, of order one or two. The implicit system obtained at each time step is solved with GMRES.

The complete one-dimensional model propellant combustion model (solid, surface, and flame) is implemented in the VULC1D code [23, 24]. Its conservation equations are semi-discretised in space using a second-order accurate finite-volume approach on a staggered grid, forming a set of index-1 differential-algebraic equations (DAEs). This specific nature has been explicitly identified [23] and requires carefully chosen time integrators so that the solution method is consistent, stable, precise and efficient. The class of ESDIRK methods [27] has proved to be well suited. Embedded schemes enable dynamic time step adaptation to optimise accuracy and efficiency.

### 3.1 Coupling methodology

The previous solvers can be coupled to compute the ignition of a combustion chamber. The underlying idea is the same as for the various large-scale ignition simulations presented since the 1990s [5, 14]. The combustion chamber is meshed in 2D or 3D and its internal flow field is simulated with the CFD solver. At each boundary face corresponding to the propellant surface, an instance of the one-dimensional propellant solver is used to compute the evolution of the thermal profile within the propellant and the combustion of the latter. At each time step of the coupled computation, the coupling variables and fluxes are exchanged between both solvers.

Following the various modelling levels presented in the Section 2, two approaches are designed. The first approach, referred to as *detailed approach*, captures the propellant flame in the fluid model. VULC1D is used to compute the evolution of the thermal profile inside the propellant and of the surface variables, but its 1D gas phase is discarded.

In the second approach, referred to as *1D flame approach*, the flame is modelled using the model from Section 2.4. Thus the CFD domain does not need to be meshed as finely near the surface, and the CFD solver can work only with inert combustion products, sparing the computational expense of evaluating chemical source terms over the whole domain. Another advantage of our approach is the ability of the 1D flame model to use a more refined representation of the propellant flame if required, for instance by including detailed transport and additional intermediate species.

To produce a time-accurate simulation of the overall combustion chamber ignition, the previous fluxes exchange must be performed periodically. This is done at each so-called coupling time step  $\Delta t$ , as depicted in Fig. 3.1. At each time step, CHARME transmits the parietal pressure and heat flux. The 1D model provides the surface variables (temperature, mass flow rate, composition) and surface fluxes which are used as boundary conditions for the fluid model.

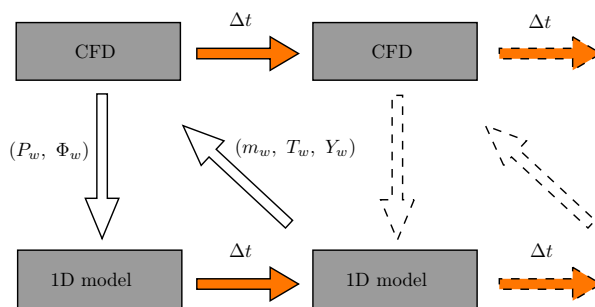


Figure 1 Coupling algorithm

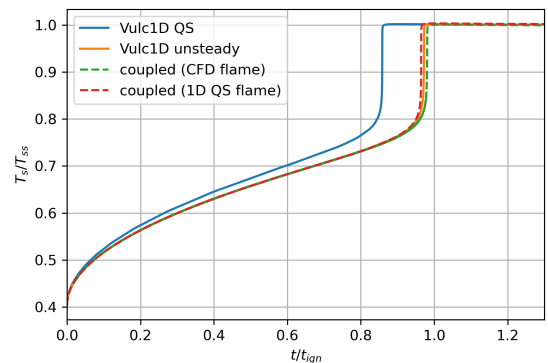


Figure 2 Surface temperature evolutions during laser-induced ignition

The coupling algorithm is first-order in time, and corresponds to a single Gauss-Seidel iteration of a waveform relaxation approach. Therefore, we only use a first-order accurate time scheme (backward Euler) in CHARME and VULC1D for the coupled simulations, and each solver only performs one time step per coupling step. Extensions of the present coupling to higher-order is the subject of ongoing research, with the added ability for each solver to perform as many substeps as required to satisfy a given error tolerance [24].

## SOLID ROCKET MOTOR IGNITION MODELLING

**3.2 One-dimensional verification**

We now verify the implementation of the previous models in a one-dimensional case of laser-induced ignition, i.e. with an additional constant heat flux imposed at the propellant surface via the term  $\Phi_{ext}$  in Eq. (6).

**3.2.1 Model parameters**

We consider a simple model of an AP-HTPB-Al propellant, which is a slight variation of the one used in [20, 23]. The solid phase is composed of the solid species  $P$  and has the following properties:  $\rho_c = 1800 \text{ kg.m}^3$ ,  $\Delta h_f^o(c) = 0 \text{ J/kg}$  at  $T = 0 \text{ K}$ ,  $c_c = 1150 \text{ J/kg/K}$ ,  $\lambda_c = 0.55 \text{ W/m/K}$ . The initial temperature is  $T_0 = 300 \text{ K}$ . At the surface, the pyrolysis mass flow rate is computed as:  $m = A_p T_s^\beta \exp(-T_{ap}/T_s)$ , with  $A_p = 1 \times 10^9 \text{ kg/s/m}^2$ ,  $\beta = 0.3$  and  $T_{ap} = 1.5 \times 10^4 \text{ K}$ . The pyrolysis process converts the solid phase into the gaseous species  $G_1$ . For the gas phase, two global species are considered: the reactant  $G_1$  and product  $G_2$ , which have the same properties except standard enthalpies. Their molar mass is  $\mathcal{M} = 27 \text{ g/mol}$ , and their heat capacities are  $c_p = 2800 \text{ J/kg/K}$ . The standard enthalpies at  $T = 0 \text{ K}$  are  $\Delta h_f^o(G_1) = 0 \text{ J/kg}$  and  $\Delta h_f^o(G_2) = -8.9 \times 10^6 \text{ J/kg}$ . The unique global reaction  $G_1 \rightarrow G_2$  is irreversible. Its reaction rate is  $\omega = A[G_1]^n T \exp(-T_a/T)$ , with  $A = 2750 \text{ s}^{-1}$ ,  $T_a = 1500 \text{ K}$ ,  $n = 0.6$  and  $[G_1]$  the concentration of  $G_1$ . The diffusion coefficients are equal for both species and taken as a linear function of  $T$  such that the Schmidt and Prandtl numbers remain constant (1 and 0.5 respectively). The thermal conductivity is  $\lambda = 0.45 \text{ W/m/K}$ .

**3.2.2 Simulation of laser-induced ignition**

The solid propellant solver has already been verified in [23] for the laser-induced ignition of a propellant sample. Thanks to the use of a fifth-order adaptive ESDIRK time scheme and a highly-refined 1D mesh, the obtained solution is very precise and can be used as a reference. The previous coupled approaches can then be tested with a similar physical configuration to verify their ability to reproduce the one-dimensional ignition.

Both the standalone VULC1D code and the coupled framework are parametrised with the previous model parameters. The gas phase is at 5 bars, and the initial temperature field is uniform at  $T = 300 \text{ K}$ , both in the solid and gas phases. The gas is initially composed only of combustion products  $G_2$  that act as the initial inert gas. For the coupled approaches, the CFD mesh has cells with a geometrical progression in thickness. For the 1D flame approach, the first CFD cell above the surface is  $10 \text{ }\mu\text{m}$  thick, which is sufficient to accurately capture the heat loss via diffusion through the gas phase during the initial heating phase. For the detailed approach, properly capturing the propellant flame in the CFD domain requires a finer mesh, thus the first cell is reduced to  $1 \text{ }\mu\text{m}$ .

At  $t = 0 \text{ s}$ , a  $1 \text{ MW.m}^{-2}$  laser heat flux is applied at the propellant surface as an additional contribution to  $\Phi_w$  in Eq. (6). The surface temperature rises, some heat being lost via conduction in the gas phase. At one point, the pyrolysis mass flow rate becomes important and a sufficient amount of gaseous reactants is expelled from the surface. They form a flame that attaches to the surface, causing a rapid increase in surface temperature. Finally, the system converges to steady state.

The obtained surface temperature evolutions are shown in Fig. 3.1. The reference result (orange curve) is obtained with VULC1D only. The blue curve is obtained with VULC1D too, but with a quasi-steady 1D gas phase. We observe that, before ignition, the temperature rises more quickly. This is due to the lack of diffusive heat loss to the gas phase, as the quasi-steady flame model results in a uniform gas temperature field at  $T = T_s$  before ignition. Therefore the point of ignition is reached more quickly, in this case 12 % faster than in the reference simulation.

The dashed curves are obtained with the two coupled approaches. The ignition time for the detailed approach (green) is 0.9% larger than the reference result, which may be attributed to the coarser gas mesh used. The red dashed curve is obtained with the 1D flame approach, with a quasi-steady flame. The heat loss at the surface via diffusion to the CFD gas phase is correctly captured, and ignition occurs 0.8% faster than in the reference simulation. This may be attributed to the faster appearance of the propellant flame, following the quasi-steady assumption.

Consequently, the quasi-steady flame assumption used for the 1D flame approach does not modify much the overall ignition behaviour. Indeed the heat loss by diffusion to the gas phase can still be captured by the direct connection between the fluid and propellant models via the heat flux  $\Phi_{ext} = \Phi_w$  in Eq. (6). Note however that the flame appearance is faster in quasi-steady mode, so there might be a more visible

difference in a configuration where the development time of the unsteady flame is not small compared to the characteristic time of ignition.

#### 4. Two-dimensional SRM test case

We wish to design a configuration that is realistic in terms of dimensions, yet simple in terms of geometrical shape. The goal is to build a reference case that makes it possible to resolve all the various phenomena (combustion, hydrodynamics, conjugate heat transfer) with high numerical accuracy via extensive mesh refinement in the CFD domain, while maintaining an affordable computational cost. Then, comparing the 1D flame approach and the detailed approach for the solid propellant combustion, the discrepancies can be confidently attributed to the differences between those two approaches, without a large impact from other sources of numerical errors, e.g. numerical dissipation.

Most 1D ignition models have been used directly on complex 2D or 3D SRMs [28, 6, 29, 14]. Also, fully documented experimental motors (geometry and propellants) are scarce in the literature. A refined modelling approach, similar to our detailed approach, has been used for the study of transient combustion and acoustic instabilities in fictitious 2D rocket motors [30, 31, 32, 33], but the ignition phase was not considered. Near-surface CFD cells were reported to be 1  $\mu\text{m}$  thick to accurately resolve the flame zone. If we are to simulate ignition with the detailed approach, we can expect that we will have to use similar grid refinements. To retain a manageable computational cost for a fully unsteady simulation, we cannot consider a 3D case. 3D simulations of the ignition of small SRM with a 1  $\mu\text{m}$  cell height at the surface, but a much coarser refinement in the longitudinal direction, have been reported [14]. The total number of cells was already on the order of 200 millions, which is far too large for the study proposed in this paper. Therefore, we choose to focus on a two-dimensional case.

We take inspiration from the fictitious axisymmetric motor TEP which has been used at ONERA for various studies, e.g. quantification of instabilities [34, 35]. The dimensions of the original TEP motor are close to those of tactical devices. The combustion chamber is 17 cm long, with an inner radius of 45 mm. The propellant grain is cylindrical and burns in a radial manner. The original configuration possesses a nozzle. Since we only focus on ignition of the propellant load, and not on the internal pressure rise dynamics, we remove the nozzle and replace it by a simple subsonic outflow condition. As we aim at studying ignition via impingement from a hot flow, we introduce an igniter in the aft-end of the motor, from which a hot jet flow enters the combustion chamber at an angle of 45 degrees with respect to the longitudinal axis, as represented by the red arrows. For simplicity, we assume the igniter jet is at chemical equilibrium, and its combustion products are the same as those of the main propellant load, but with a lower temperature. The introduction of an igniter jet leads to a complex flow field which features flow instabilities and recirculation areas. This renders the test case very sensitive to the propellant surface dynamics. In particular, it can highlight differences in behaviours between various ignition models, making it a demanding test case, able to show discrepancies between the dynamics of different models for the solid propellant combustion.

To simplify the configuration, the nozzle is removed, and the nozzle entrance plane is replaced by a subsonic outflow condition. The resulting configuration is axisymmetric and has been used in a previous study [36]. Although good first results were obtained in comparing both approaches on this configuration, issues arose with pressure waves generated by the start-up of the igniter jet. These reflect multiple times on both the axisymmetric and the right exit boundary conditions and come back to the surface of the propellant. We have observed that this phenomenon is the root cause of an exacerbated sensitivity of the overall simulation result with respect to the CFD mesh refinement, due to intricate interactions between the flow field, acoustics, surface combustion, and numerical stability.

To avoid such issues, we have modified the configuration so as to discard these pressure-induced interactions. The 2D axisymmetric configuration is replaced by a planar 2D one, where the upper (formerly the symmetry condition) and right exit boundary conditions both correspond to subsonic outflow conditions and are pushed much further away from the propellant flame zone with a gradual mesh coarsening. Thanks to this modification, pressure wave reflections do not occur within the time range of interest, leading to a less disturbed unsteady solution. The modified configuration is sketched in Figure 3.

## SOLID ROCKET MOTOR IGNITION MODELLING

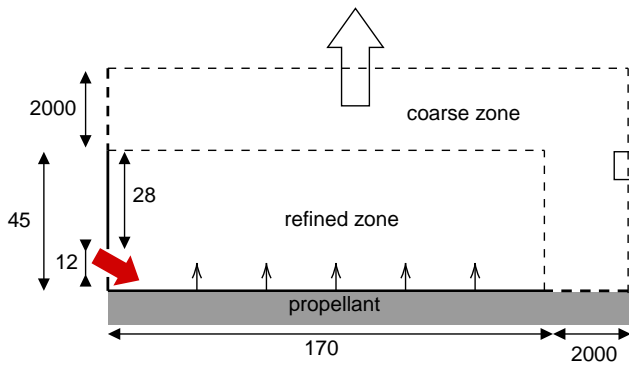


**Figure 3** Sketch of the 2D test case

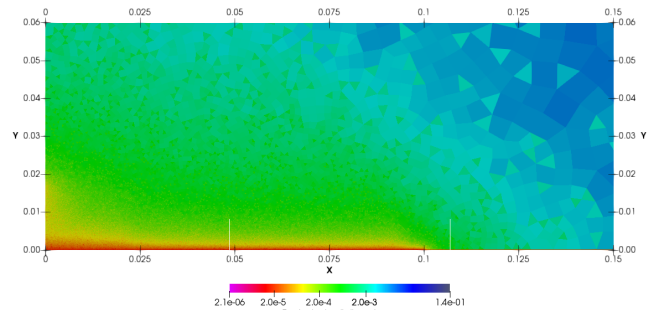


**Figure 4** Field of equivalent cell diameter (m) for the fine mesh

#### 4.1 Boundary and initial conditions

The fluid domain is 2D plane and rectangular. The left boundary is an adiabatic wall boundary, with an opening near the bottom, through which the igniter flow is injected at  $T = 2300$  K with a mass flow rate of  $110 \text{ kg}\cdot\text{m}^2\cdot\text{s}^{-1}$  and an angle of 45 degrees. The igniter injection hole starts at  $y = 5$  mm and is 12 mm long. The igniter flow is maintained during the whole simulation. The injected flow is turbulent and the associated scalars are  $k = 100$  J/kg, and  $\omega = 1.8 \times 10^4$   $\text{s}^{-1}$ . The velocity in the core of the established igniter jet is approximately 200 m/s.

The right and upper boundaries (only visible in the sketch) are located at  $x = 2$  m and  $y = 2$  m respectively. They are subsonic outflow conditions, with a prescribed pressure of 0.5 MPa. The lower boundary is a solid propellant boundary. Each of its faces is associated with one instance of the one-dimensional model, solved with the VULC1D code following the approach described in Section 3.1. The zone of particular interest is the portion of the surface propellant between  $x = 0$  m and  $x = 0.1$  m. When the surface is ignited, the combustion products are injected with no turbulent kinetic energy ( $k = 0$ ) and  $\omega = 1.8 \times 10^3$   $\text{s}^{-1}$ .

The initial fluid state is uniform at 0.5 MPa,  $T = 293$  K, zero velocity and turbulent kinetic energy. The solid propellant thermal profile is initialised at the same temperature. We use the same physico-chemical modelling as presented in Section 3.2.1. Initially, only combustion products  $G_2$  are present in the CFD and (if active) in the 1D gas domains. The igniter flow also injects the same combustion products. In the CFD domain, the reactant species  $G_1$  only appears near the surface when the detailed coupling is employed.

#### 4.2 Spatial discretisation

The domain is discretised in an unstructured manner with quadrangles and triangles and is highly refined in the igniter flow. To control the mesh refinement near the propellant surface, a small zone above the propellant (200  $\mu\text{m}$  thick in the  $y$ -direction) is meshed in a cartesian manner. For the detailed approach in particular, this part of the CFD mesh must be properly refined to capture the flame profile. A reference mesh is constructed where the first layer of cells above the propellant has a thickness  $\delta = 1$   $\mu\text{m}$  in the  $y$ -direction, perpendicular to the propellant surface. In the structured part of the mesh, the cell thickness slowly increases in a geometrical fashion as we move away from the propellant. Thus, the near-surface hydrodynamics, conjugate heat transfer and, in the case of the detailed approach, the gaseous propellant flame, can be resolved with great spatial accuracy. The field of equivalent diameter of the mesh cells is plotted in Figure 4 for this mesh. This diameter  $d$  is defined as:  $d = 2\sqrt{S/\pi}$ , i.e. it is the diameter of a disc that would have the same area  $S$  as the cell considered.

Properly resolving the conjugate heat-transfer at the propellant surface requires a sufficient near-surface mesh refinement. This is generally verified with the criteria  $y_1^+ \leq 1$ , with  $y_1^+$  the dimensionless height of the first cell above the surface [37], defined as  $y_1^+ = y_1 u_\tau / \nu$ , with  $y_1$  the height of the first cell,  $\nu = \mu/\rho$  the kinematic viscosity,  $u_\tau = \sqrt{\tau_w/\rho_w}$  the friction velocity where the wall shear stress is  $\tau_w = \rho_w \nu (d_y u)_w$ . A large amount of numerical work can be found in the literature, and the commonly accepted criteria for a proper spatial resolution of the boundary layer is  $y_1^+ \leq 1$ . *A posteriori* analysis of our simulation results have shown that setting  $\delta = 1$   $\mu\text{m}$  yields  $y_1^+ < 0.2$  over the propellant, hence the boundary layer is correctly

resolved. Figure 5 shows the mesh and the propellant flame near the ignition front for the detailed approach. We can clearly observe the gradual mesh refinement near the surface, and the transition to the unstructured mesh for the rest of the domain.

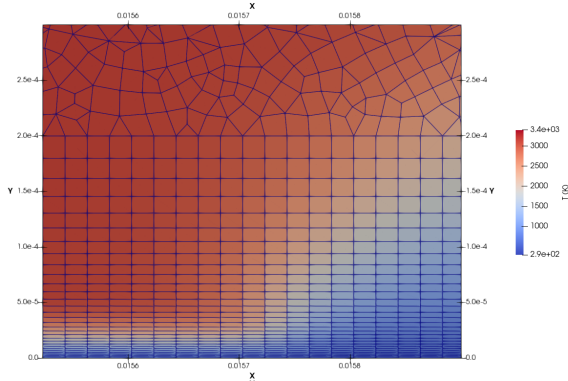


**Figure 5** Details of the fine mesh

name	$\delta$ ( $\mu\text{m}$ )	$\Delta x$ ( $\mu\text{m}$ )	number of CFD cells
fine	1	20	$3.48 \times 10^5$
medium	4	20	$2.92 \times 10^5$
coarse	20	20	$2.42 \times 10^5$

**Table 1** Main characteristics of the 3 meshes

To accurately capture the lateral flame propagation, the propellant surface is discretised with a uniform cell length  $\Delta x = 20 \mu\text{m}$  for  $x \in [0, 0.1]$  m, i.e. there are 5000 mesh faces in this zone. From  $x = 0.1$  m to  $x = 2$  m,  $\Delta x$  is gradually increased, such that only 97 additional boundary faces are required. Each of the 5097 boundary faces is associated with an instance of the one-dimensional model. Each 1D propellant model is discretised with 60 cells for the solid phase and 200 cells for the 1D flame (if activated).

When using the 1D flame model, the near-surface mesh refinement can be relaxed. Thus, an intermediate mesh is constructed with  $\delta = 4 \mu\text{m}$ . Simulation results show that  $y_1^+ < 0.7$ , hence the conjugate heat transfer should also be properly resolved. To study the effect of the near-surface mesh resolution, another mesh was created, with the first cell height set to  $20 \mu\text{m}$ , all other parameters being unmodified. The resulting coarse mesh yields  $y_1^+ < 4$ . The 3 meshes only differ by the vertical geometric progression inside the structured layer. They all have the same cell height and width at the top of the structured layer, and the same near-surface lateral refinement, hence the unstructured mesh is unaffected. Their main characteristics are summarised in Table 1.

### 4.3 Numerical setup

The coupled integration of VULC1D and CHARME is performed using the first-order coupling algorithm described in Section 3. CHARME uses a linearised implicit Euler scheme solved with GMRES, while VULC1D uses the fully nonlinear implicit Euler scheme. The coupling time step is taken as the CFD time step from CHARME.

## 5. Reference result obtained with the detailed approach

A first simulation is run on the fine mesh with the detailed approach. A constant time step  $\Delta t = 2 \times 10^{-8}$  s is used, such that the unsteady evolution is precisely resolved, even with the first-order temporal scheme. Thus, this simulation is termed as “reference” since all the flow field dynamics can be considered as properly resolved, both in terms of spatial and temporal discretisations. In this section, we analyse the evolution of the chamber flow field and propellant surface.

Various snapshots of the temperature flow field are shown in Figure 6 for the reference simulation. The initial impingement of the igniter jet is clearly visible, as well its progression above the propellant surface. From the third snapshot ( $t = 3$  ms) onwards, an ignited zone appears around  $x = 0.01$  m, and a second ignited zone appears in the last snapshot ( $t = 5$  ms) between  $x = 0.04$  m and  $x = 0.05$  m.

The first ignited zone produces a strong parietal injection which deflects the igniter jet away from the propellant surface, creating a recirculation zone ahead of the ignition front. This effect is also exacerbated by the two-dimensional configuration.

### 5.1 Near-surface flow

Let us focus on the zone of igniter impingement. Figure 7 shows the flow field near the ignited zones at  $t = 5$  ms for the reference simulation. The igniter jet flow and the flow coming from the ignited surfaces are

## SOLID ROCKET MOTOR IGNITION MODELLING

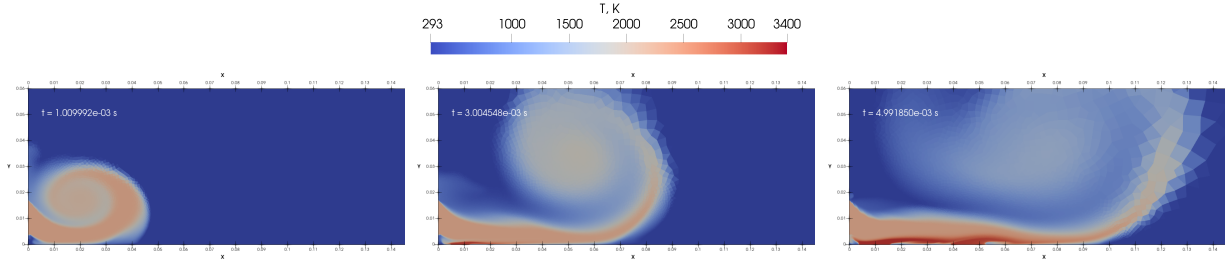


**Figure 6** Evolution of the temperature field in the reference simulation

clearly distinguishable, as seen from the temperature and flow direction discrepancies. At the ignited surface, the flow field coming from the surface pyrolysis is accelerated via thermal expansion in the propellant flame. Initially vertical, its direction quickly changes due to the interaction with the igniter jet. This flow turning is already slightly apparent in the flame zone, see Figure 9a. The flame is therefore slightly bent, which should in theory lead to an increased wall heat flux compared to the unbent case. The angle of the flow velocity vector with respect to the vertical is however very limited in the flame zone ( $< 0.1$  deg), therefore simple geometrical considerations show that the increase of the heat flux normal to the surface is on the order of 0.01% compared to the unbent case, hence is insignificant. The turbulent viscosity  $\mu_t$  has also been analysed in this region and is completely negligible in the whole flame zone. Therefore, no turbulent enhancement of the parietal heat transfer occurs with the detailed approach, as tacitly assumed in the 1D flame model.

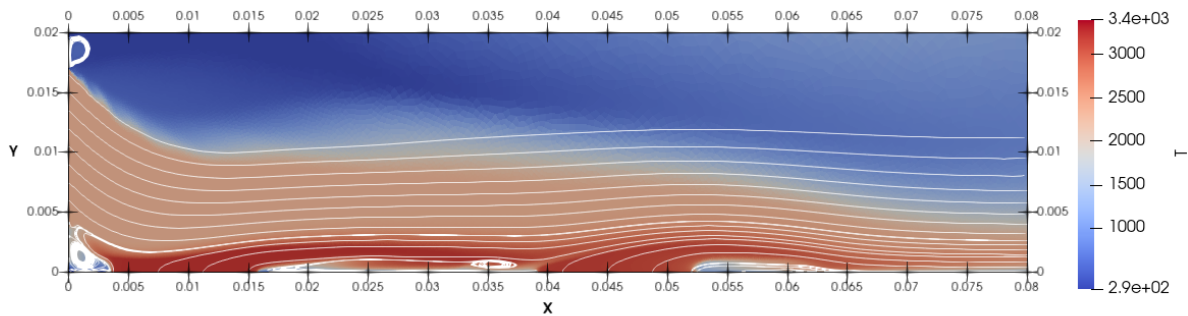


**Figure 7** Temperature field and streamlines around the ignited zones at  $t = 5$  ms

## 5.2 Ignition dynamics

To better visualize the heating of the propellant surface and the propagation of ignition, Figure 8a shows the space-time diagram of the surface temperature for the reference simulation, while Figure 8b shows the space-time diagram of the heat flux ( $\lambda_c \partial_\eta T$ ) ( $0^-$ ) that enters the solid phase. These visualisations give a clear representation of the ignited zones and of the temporal evolution of the grain heating.

The igniter jet impinges the surface at  $t = 0.4$  ms and  $x = 7.8 \times 10^{-3}$  m, as indicated by the first surface temperature increase. The first ignition occurs at  $t = 2.4$  ms at the same location. Ignition then propagates around this point, thanks to the heat already accumulated in the solid propellant and to the increased heat flux caused by the propellant flame. The propellant combustion products that are expelled by the first ignited zone are quickly convected inside the lower part of the igniter jet, which leads to a temporary increase of the wall heat flux in the neighbourhood of the first ignited point, revealed by the thin, nearly horizontal, cyan ( $\Phi_w \approx 10$  MW.m $^{-2}$ ) line in Figure 8b, starting from the point of first ignition.

The igniter jet is deflected by the pyrolysis mass flow rate from the first ignited zone, and thus a portion of the propellant surface is isolated from the convective heat transfer, as seen by the low-flux region near  $x = 25$  mm and  $t = 4$  ms.

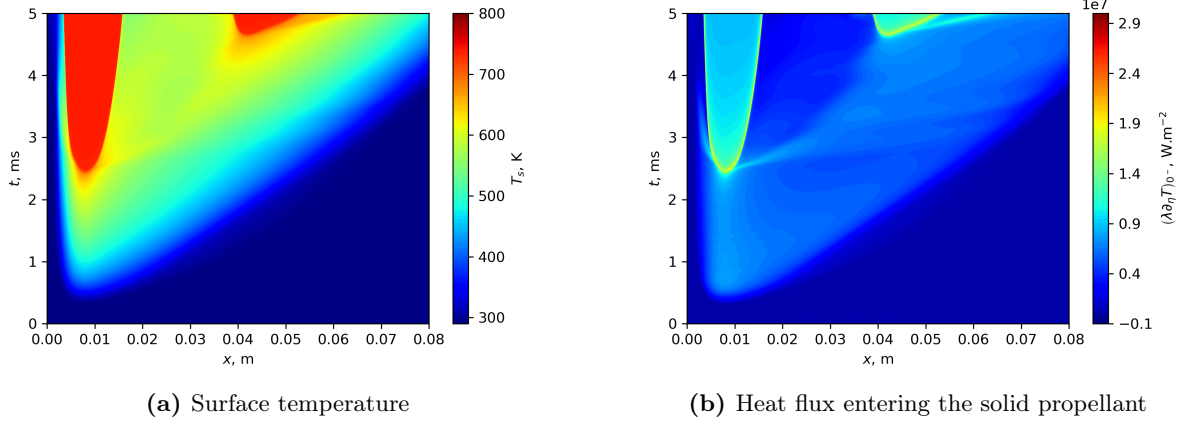


**Figure 8** Evolution of the propellant surface for the reference simulation

## 6. Comparison of both modelling approaches

We now compare the previous reference simulation with the results obtained using the 1D flame approach. A simulation with the latter approach is conducted on the intermediate mesh with the same time step  $\Delta t = 2 \times 10^{-8}$  s, and for the same physical time of 5 ms. To study the effect of the CFD mesh refinement, another simulation is run on the coarse mesh with the 1D flame approach and the same settings. The overall flow field evolutions are quite similar, hence a comparison with Figure 6.

### 6.1 Near-surface flow

In Figure 9, the velocity field near the surface inside the first ignited zone at  $t = 5$  ms is plotted for these 2 simulations and the reference simulation. We see that the streamlines are very similar, and the velocity magnitudes in the upper layer of the boundary flow are in very good agreement. The only major difference is the effect of the thermal expansion in the case where the flame is solved within the CFD model. With the 1D flame approach, this thermal expansion is already accounted for in the 1D flame model and therefore is not visible in the CFD solution. The similarity between the solution profiles is a very good *a posteriori* verification that the propellant flame can be concentrated in a boundary model instead of being solved within the CFD model, without much effect on the overall result.

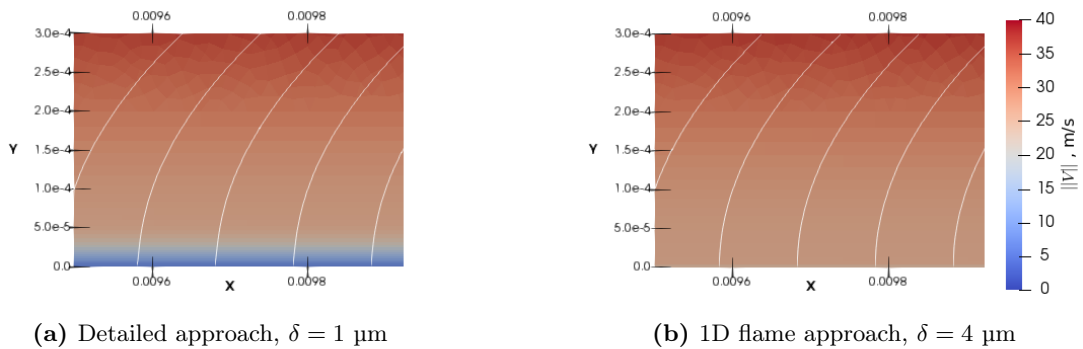


**Figure 9** Velocity field near  $x = 0.01$  m at  $t = 5$  ms

### 6.2 Surface evolution

To better visualize the heating of the propellant surface and the propagation of ignition, Figures 10a, 10b and 10c show space-time diagrams of the evolution of the surface temperature for each simulation. This allows for a clear representation of the ignited zones and of the temporal evolution of the grain heating.

## SOLID ROCKET MOTOR IGNITION MODELLING

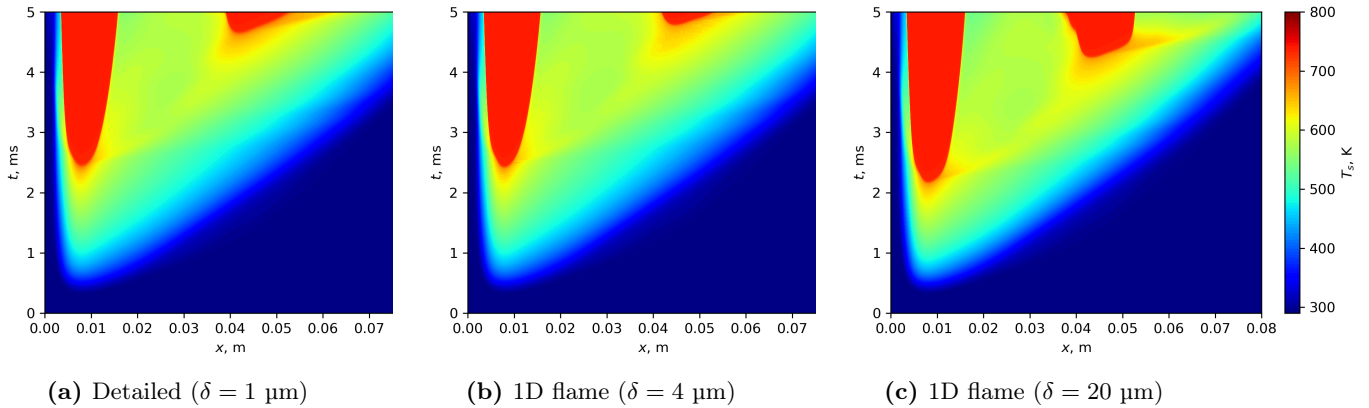


**Figure 10** Surface temperature evolution

First, we can observe that all results are overall in excellent agreement for the first 4 ms. In the case of the 1D flame approach with the intermediate mesh, ignition occurs at the same time and location ( $t = 2.4$  ms and  $x = 7.8 \times 10^{-3}$  m) as for the reference simulation. For the 1D flame approach with the coarse mesh, ignition occurs slightly sooner at  $t = 2.15$  ms and at the same location, i.e. the near-surface mesh resolution has a strong impact on the occurrence of first ignition. A more detailed analysis has shown that during the heating phase, the heat flux ( $\lambda_c \partial_\eta T$ ) ( $0^-$ ) is roughly 10 % larger in average in the simulation with  $\delta = 20 \mu\text{m}$  compared to the other simulations. This indicates that the conjugate heat-transfer is not well-resolved with the coarse mesh.

The first ignited zone produces a strong parietal injection which deflects the igniter jet away from the propellant surface. This creates a recirculation zone ahead of the ignition front, which also increases the overall sensitivity of the surface ignition, because the recirculation zone is very little exposed to the convective heat transfer from the igniter flow.

A second ignition zone appears near  $t = 5$  ms and  $x = 5 \times 10^{-2}$  m in all simulations. The detailed model on the fine mesh and the 1D flame model on the intermediate mesh have a very similar development for this zone, although ignition occurs slightly sooner with the detailed model. On the coarse mesh however, ignition of the second zone occurs much sooner. This can be once more attributed to the poorer resolution of the conjugate heat-transfer. Also, since the first zone ignites earlier, the jet deflection is not the same, and the point where the igniter jet once again impinges the surface (having incorporated some hotter gases from the propellant combustion in the first zone) is different. Consequently, the heating of the downstream unignited regions is modified and the secondary ignition zone appears at slightly different times and locations. This effect is also exacerbated by the two-dimensional configuration, because the recirculation zone cannot be circumvented.

Overall, we see that the 1D flame approach yields quantitatively very similar results compared to the detailed approach if the CFD mesh is sufficiently refined. If a coarse mesh is used, the discrepancies can be attributed to a poorer resolution of the chamber fluid model hydrodynamics and conjugate heat transfer.

## Conclusion

A new strategy for the simulation of solid rocket motor ignition has been presented. Two approaches have been designed, which differ by their representations of the gaseous flame. The detailed approach directly captures this flame within the CFD solver used for the chamber flow, while the 1D flame approach models it as a boundary phenomenon which is solved in 1D. Compared to the existing ignition models, the specificity of our 1D flame approach lies in the numerical resolution of the propellant flame, which allows for a nearly arbitrary level of modelling to be employed, without resorting to very simplified flame models. Also, the transition to ignition occurs dynamically, which may lead to better fidelity across a wider variety of conditions than a simpler temperature criterion.

Both approaches have been verified on the case of 1D laser-induced ignition and they produce results in agreement with those obtained with a purely 1D approach. To study the ignition dynamics of a propellant surface in a setting that is more representative of actual motors, a 2D test case has been designed to feature the various phenomena encountered in SRMs: igniter jet impingement, complex hydrodynamics, flame spread.

This case has proven to be highly sensitive, in particular due to the stringent near-surface mesh refinement required. Also, the two-dimensional setting allows for sustained recirculation zones to be created, isolating part of the unignited propellant surface from the igniter jet, and this effect is dependent on the propellant ignition, flame spread and mass flow rate distribution.

The 1D flame approach and the detailed approach yield nearly identical results on fine meshes. This clearly demonstrates the accuracy of the 1D flame approach, even in highly-transient and multidimensional simulations. Overall, this configuration gives a strong demonstration that the 1D flame model behaves correctly, and that it is a sensible modelling approach for large-scale ignition transient simulations. This study legitimates the widespread use of such a modelling as in all SRM ignition simulations reported in the literature.

Coarsening the CFD mesh has a noticeable impact on the conjugate heat transfer, causing an overall faster heating of the propellant when the criterion  $y_1^+ \leq 1$  is not met. Future work should investigate the use of wall laws to improve the accuracy of the conjugate heat transfer on a coarser near-surface mesh, which would greatly benefit the 1D flame approach. This is a prerequisite for legitimating the use of the 1D flame approach on larger 3D SRM geometries without a costly near-surface mesh refinement.

Further studies with various lateral and vertical near-surface mesh refinements should be conducted to assess the effect of spatial resolution on the flame spread. Radiation models available in CEDRE can be added to the overall modelling to account for gas and surface radiation. This will allow for radiative grain preheating to occur, which may soften the differences observed in the 2D test case, as radiation has often been reported to be an important contribution for the propagation of ignition [28].

Some aspects remain difficult to model with the 1D flame approach. For instance, at the aft-end of an SRM, turbulence may impact the flame structure [30] and thus the burning rate of the propellant. Our current 1D flame model does not account for any turbulence related effects. The inclusion of turbulence-related conservation equations in the 1D flame model could improve this aspect by providing an unsteady numerical wall law. The detailed approach could be used to study fine flame-flow interactions, such as these turbulence effects, or combustion response to high-frequency pressure oscillations.

Finally, the presented coupling strategy is only first-order accurate in time. Both the CFD and propellant codes are however able to achieve higher-order separately. Future work should focus on implementing the adaptive coupling framework explored in [24] to improve the efficiency and accuracy of the coupling.

## Acknowledgments

The present research was conducted thanks to a Ph.D grant co-funded by DGA, Ministry of Defence (E. Faucher, Technical Advisor), and ONERA.

## References

- [1] K. Parker and M. Summerfield. The ignition transient in solid propellant rocket motors. In *Solid Propellant Rocket Conference*, 1964.
- [2] S. Desoto and H.A. Friedman. Flame spreading and ignition transients in solid grain propellants. *AIAA Journal*, 3(3):405–412, 1965.
- [3] A. Peretz, K.K. Kuo, L.H. Caveny, and M. Summerfield. Starting transient of solid-propellant rocket motors with high internal gas velocities. *AIAA Journal*, 11(12):1719–1727, 1973.
- [4] L. d’Agostino, L. Biagioni, and G. Lamberti. An ignition transient model for solid propellant rocket motors. In *37th Joint Propulsion Conference and Exhibit*, 2001.
- [5] W.A. Johnston. Solid rocket motor internal flow during ignition. *Journal of Propulsion and Power*, 11(3):489–496, 1995.
- [6] P. Alavilli, J. Buckmaster, T.L. Jackson, and M. Short. Ignition-transient modeling for solid propellant rocket motors. In *36th AIAA/ASME/SAE/ASSE Joint Propulsion Conference and Exhibit*, 2000.
- [7] C. Koren, R. Vicquelin, and O. Gicquel. Self-adaptive coupling frequency for unsteady coupled conjugate heat transfer simulations. *International Journal of Thermal Sciences*, 118:340 – 354, 2017.

## SOLID ROCKET MOTOR IGNITION MODELLING

- [8] E. Radenac, J. Gressier, and P. Millan. Methodology of numerical coupling for transient conjugate heat transfer. *Computers and Fluids*, 100:95 – 107, 2014.
- [9] W. Erikson and M. Beckstead. Modeling unsteady monopropellant combustion with full chemical kinetics. In *36th AIAA Aerospace Sciences Meeting and Exhibit*, 1998.
- [10] K. Meredith, M. Gross, and M. Beckstead. Laser-induced ignition modeling of HMX. *Comb. and Flame*, 162, 09 2014.
- [11] S. Gallier, A. Ferrand, and M. Plaud. Three-dimensional simulations of ignition of composite solid propellants. *Combustion and Flame*, 173:2–15, 11 2016.
- [12] N. Meynet. *Simulation numérique de la combustion d’un propergol solide*. PhD thesis, Université Pierre et Marie Curie, 2005.
- [13] M. Brandyberry, R. Fiedler, and C. McLay. Verification and validation of the rostar 3-d multi-physics solid rocket motor simulation program. In *41st AIAA/ASME/SAE/ASSE Joint Propulsion Conference and Exhibit*, 2005.
- [14] Q. Li, P. Liu, and G. He. Fluid-solid coupled simulation of the ignition transient of a solid rocket motor. *Acta Astronautica*, 110:180 – 190, 2015. Dynamics and Control of Space Systems.
- [15] Y.K. Li, X. Chen, J. Xu, C. Zhou, and O. Musa. Three-dimensional multi-physics coupled simulation of ignition transient in a dual pulse solid rocket motor. *Acta Astronautica*, 146:46–65, 2018.
- [16] M. Salita. Modern SRM ignition transient modeling. I-Introduction and physical models. In *37th Joint Propulsion Conference and Exhibit*, 2001.
- [17] A. Bizot. Ignition and unsteady combustion of AP-based composite propellants in subscale solid rocket motors. *International Journal of Energetic Materials and Chemical Propulsion*, 4(1-6):1046–1061, 1997.
- [18] O. Orlandi, F. Fourmeaux, and J. Dupays. Ignition study at small-scale solid rocket motor. In *8th European Conference for Aeronautics and Space Sciences (EUCASS)*, 2019.
- [19] F. Menter. Two-equation eddy-viscosity turbulence models for engineering applications. *AIAA Journal*, 32:1598–1605, 1994.
- [20] L. François, J. Dupays, D. Davidenko, and M. Massot. Travelling wave mathematical analysis and efficient numerical resolution for a one-dimensional model of solid propellant combustion. *Combustion Theory and Modelling*, 24(5):775–809, 2020.
- [21] V. Giovangigli, N. Meynet, and M.D. Smooke. Application of continuation techniques to ammonium perchlorate plane flames. *Combustion Theory and Modelling*, 10(5):771–798, 2006.
- [22] D.A. Smith. *Modeling Solid Propellant Ignition Events*. PhD thesis, Brigham Young University, 2011.
- [23] L. François, J. Dupays, D. Davidenko, and M. Massot. Solid propellant combustion in the low Mach one-dimensional approximation: from an index-one differential-algebraic formulation to high-fidelity simulations through high-order time integration with adaptive time-stepping. hal-02888035 v1, 2021.
- [24] L. François. *Multiphysics modelling and simulation of solid rocket motor ignition*. PhD thesis, Institut Polytechnique de Paris, 2022.
- [25] A. Refloch, B. Courbet, A. Murrone, P. Villedieu, C. Laurent, P. Gilbank, J. Troyes, L. Tessé, G. Chainéray, J.-B. Dargaud, E. Quémérais, and F. Vuillot. Cedre software. *AerospaceLab Journal*, pages 1–10, 2011.
- [26] C. Le Touze. *Couplage entre modèles diphasiques à “phases séparées” et à “phase dispersée” pour la simulation de l’atomisation primaire en combustion cryotechnique*. PhD thesis, Université Nice Sophia Antipolis, 2015.
- [27] A. Kvaerno. Singly diagonally implicit Runge-Kutta methods with an explicit first stage. *BIT*, 44:489–502, 08 2004.

- [28] P. Le Helley. 3D turbulent Navier-Stokes simulations of ignition transients in solid rocket motors. In *34th AIAA/ASME/SAE/ASSE Joint Propulsion Conference and Exhibit*, 1998.
- [29] Q. Li, G.G. He, P.J. Liu, and J. Li. Coupled simulation of fluid flow and propellant burning surface regression in a solid rocket motor. *Computers and Fluids*, 93:146–152, 2014.
- [30] I.S. Tseng and V. Yang. Combustion of a double-base homogeneous propellant in a rocket motor. *Combustion and Flame*, 96(4):325–342, 1994.
- [31] T.S. Roh, I.S. Tseng, and V. Yang. Effects of acoustic oscillations on flame dynamics of homogeneous propellants in rocket motors. *Journal of Propulsion and Power*, 11(4):640–650, 1995.
- [32] T.S. Roh, S. Apte, and V. Yang. Transient combustion response of homogeneous solid propellant to acoustic oscillations in a rocket motor. *Symposium (International) on Combustion*, 27(2):2335–2341, 1998.
- [33] S. Apte and V. Yang. Unsteady flow evolution and combustion dynamics of homogeneous solid propellant in a rocket motor. *Combustion and Flame*, 131(1-2):110–131, 2002.
- [34] N. Lupoglazoff and F. Vuillot. Simulation numérique bidimensionnelle des écoulements instationnaires dans les propulseurs  $\tilde{A}$  propergol solide. *La Recherche Aéronautique*, 2:21–41, 1992.
- [35] E. Daniel, N. Lupoglazoff, F. Vuillot, T. Basset, and J. Dupays. 2D Navier-Stokes stability computations for solid rocket motors - Rotational, combustion and two-phase flow effects. In *33rd Joint Propulsion Conference and Exhibit*, 1997.
- [36] L. François, J. Dupays, and M. Massot. A new simulation strategy for solid rocket motor ignition: coupling a CFD code with a one-dimensional boundary flame model, verification against a fully resolved approach. In *AIAA Propulsion and Energy 2021 Forum*, 2021.
- [37] S.B. Pope. *Turbulent Flows*. Cambridge University Press, 2000.